PHOTONICS Research

Routing emission with a multi-channel nonreciprocal waveguide

Hao Hu,[1] Liangliang Liu,[1,2,4] Xiao Hu,[1] Dongjue Liu,[1] and Dongliang Gao[3,5]

[1]School of Electrical and Electronic Engineering, Nanyang Technological University, 639798 Singapore, Singapore
[2]Research Center of Applied Electromagnetics, School of Electronic and Information Engineering, Nanjing University of Information Science and Technology, Nanjing 210044, China
[3]School of Physical Science and Technology, Collaborative Innovation Center of Suzhou Nano Science and Technology, Soochow University, Suzhou 215006, China
[4]e-mail: llliu@ntu.edu.sg
[5]e-mail: dlgao@suda.edu.cn

Received 8 January 2019; revised 17 March 2019; accepted 4 April 2019; posted 5 April 2019 (Doc. ID 356838); published 16 May 2019

In this work, we present a multi-channel nonreciprocal waveguide, which is composed of a gyrotropic-bounded dielectric on the bottom and a plasmonic material on the top. The Lorentz reciprocity in the time-invariant system is broken when applying an external static magnetic field on the gyrotropic material. The nonreciprocal emission from the dipole source located in the center of the waveguide is observed in extended waveband channels. The proposed heterostructure serves as a photonic dichroism once the dielectric is replaced by a nonlinear material. The associated second harmonic generated in the nonlinear process can be separated from the fundamental signal under proper magnetic field intensity. Our findings may provide significant guidance for designing nonreciprocal photonic devices with superiorities of a tunable waveband, multiple channels, and small footprint.

https://doi.org/10.1364/PRJ.7.000642

1. INTRODUCTION

An asymmetric system based on gyrotropic material allows manipulation of electromagnetic (EM) wave scattering, transmission, and propagation in a nonreciprocal and tunable manner [1–5]. The nonreciprocal property of the light–matter interaction has been intensely studied with the development of nontrivial physical phenomena (e.g., breaking the time-bandwidth limit) [6] and nonreciprocal photonic devices (e.g., optical diode and circulator) [7,8]. More importantly, the time-reversal symmetry broken by the gyrotropic material in the external static magnetic field has vast potential for the realization of photonic topological insulators [9,10], which is a promising material and a current research hotspot.

Nonreciprocal behaviors of Cherenkov radiation and dipole emission in a half-plane gyrotropic material have been investigated in recent work [11,12]. In these systems, the surface plasmon polaritons (SPPs) are excited directionally around the associated plasmon resonances. Therefore, the directional propagation of the EM modes is stringently dependent on the operation wavelength [13–17]. Due to the single boundary between the gyrotropic material and the adjacent dielectric, only one surface mode can be supported in each propagation direction. This inevitably restricts the freedoms of the nonreciprocal devices owing to the limited working channels. In this work, we find that the working channels can be multiplied by adopting the gyrotropic-based heterostructure. A plasmonic material (e.g., metals) is added on the top of the dielectric loaded with a gyrotropic material. The EM modes induced on the surfaces of the plasmonic material and gyrotropic material can be strongly coupled to each other, and thus generate nonreciprocal supermodes when their coupling strength is larger than the dissipation of the system [18,19]. These nonreciprocal supermodes can extend the waveband channels for additional nonreciprocal operations.

Moreover, it is a hot research topic currently to enhance and separate the coherent high-order harmonic produced during the nonlinear process with strategies such as backward phase matching in negative-index materials [20–26]. But the conditions of strategies such as backward phase matching are rather strict, requiring a unique dispersion relation of the materials and a specific wavevector of the incidence (e.g., $n(\omega) = -n(2\omega)$, $2k(\omega) = k(2\omega)$, where n is the refractive index and k is the wavevector [23]). Thus, the perturbation of the incidence angle can drastically deteriorate nonlinear conversion efficiency. In this paper, we show that the extraction of nonlinear signal by adopting the nonreciprocal system can overcome the previous problem. The propagation direction of the EM mode at a given wavelength is intrinsically determined by the nonreciprocity of the asymmetric system, but unrelated to the wavevector of the source. Thus, the high-order harmonic and the fundamental signal can be separated by tuning the fundamental frequency to an appropriate one. Furthermore, we show that when the transparent dielectric is replaced by a second-order nonlinear material in our multi-channel nonreciprocal system, the second harmonic can be emitted and propagate antiparallelly to the fundamental signal in two different working wavebands, enhancing the freedom of the photonic dichroism.

2. MODEL AND THEORY

The nonreciprocal waveguide is constructed with a transparent dielectric slab with a thickness of $2d$, loaded between a plasmonic material and a gyrotropic material, as shown in Fig. 1(a). The dielectric function of the gyrotropic material in the static magnetic field $\mathbf{B}$ is expressed as [2,6,25]

$$\bar{\bar{\varepsilon}} = \epsilon_{\infty 1}\begin{bmatrix} \varepsilon_t & -\mathrm{i}\varepsilon_g & 0 \\ \mathrm{i}\varepsilon_g & \varepsilon_t & 0 \\ 0 & 0 & \varepsilon_a \end{bmatrix}, \tag{1}$$

where $\epsilon_t = 1 - \frac{\omega_{p1}^2(\omega+\mathrm{i}\gamma_1)}{\omega(\omega+\mathrm{i}\gamma_1)^2-\omega\omega_c^2}$, $\epsilon_g = \frac{1}{\omega}\frac{\omega_c\omega_{p1}^2}{\omega_c^2-(\omega+\mathrm{i}\gamma_1)^2}$, and $\epsilon_a = 1 - \frac{1}{\omega}\frac{\omega_{p1}^2}{\omega+\mathrm{i}\gamma_1}$. Particularly, ω is the operation frequency of the incident light, ω_c is the cyclotron frequency and proportional to the magnetic field of the incident light, $\omega_{p1} = 2 \times 10^{15}$ rad/s is the plasmon frequency of the gyrotropic material, $\gamma_1 = 0.01\omega_{p1}$ is the corresponding collision frequency, and $\epsilon_{\infty 1} = 1$ is high-frequency permittivity. Meanwhile, the polarization of magnetic field $\mathbf{B}$ is along the z direction. The dielectric function of the plasmonic material is given by the Drude model as [26]

$$\varepsilon_m = \epsilon_{\infty 2}\left[1 - \frac{\omega_{p2}^2}{\omega(\omega+\mathrm{i}\gamma_2)}\right]. \tag{2}$$

Here, we assume that the plasmon frequency $\omega_{p2} = 1.1\omega_{p1}$, collision frequency $\gamma_2 = 0.01\omega_{p2}$, high-frequency permittivity $\epsilon_{\infty 2} = 1$, and relative permittivity of the dielectric medium is $\epsilon_d = 5$. The thickness of the dielectric is set as $2d = 50$ nm to make the coupling strength of the EM modes larger than

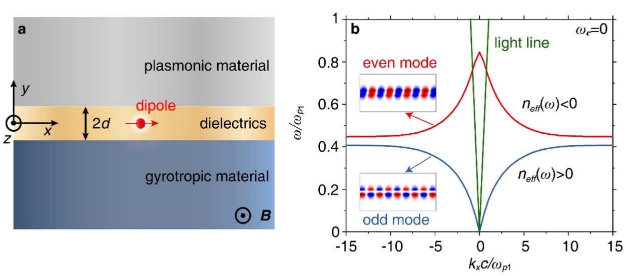

Fig. 1. (a) Schematic diagram of the multi-channel nonreciprocal waveguide, which is composed of a plasmonic material, a dielectric, and a gyrotropic material. A static magnetic field $\mathbf{B} = B\hat{\mathbf{z}}$ with the polarization along the z direction is applied to the gyrotropic material. A dipole with x-oriented dipole momentum is located in the center of the transparent dielectric with a thickness of $2d = 50$ nm. (b) Dispersion relation of the proposed waveguide when the cyclotron frequency $\omega_c = 0$ (zero magnetic field). The insets are the E_x-field distribution of the odd mode and even mode, respectively.

the loss rate of the system [18,19]. In the end, the strong coupling between the EM modes on the adjacent interfaces leads to the formation of supermodes [i.e., the even mode and odd mode shown in Fig. 1(b)].

In a source-free system, the tangent field components in the frequency domain are of the form [11]

$$H_z^f = \begin{cases} \int \mathrm{d}k_x C_{\mathrm{TM}}^{+} \mathrm{e}^{\mathrm{i}k_y^m y} \mathrm{e}^{\mathrm{i}k_x x} & y > d \\ \int \mathrm{d}k_x (B_{\mathrm{TM}}^{+} \mathrm{e}^{\mathrm{i}k_y^d y} + B_{\mathrm{TM}}^{-} \mathrm{e}^{-\mathrm{i}k_y^d y}) \mathrm{e}^{\mathrm{i}k_x x} & -d < y < d, \\ \int \mathrm{d}k_x C_{\mathrm{TM}}^{-} \mathrm{e}^{\mathrm{i}k_y^g y} \mathrm{e}^{\mathrm{i}k_x x} & y < -d \end{cases} \tag{3}$$

$$E_x^f = -\frac{1}{\omega\varepsilon_0}\begin{cases} \int \mathrm{d}k_x S_m C_{\mathrm{TM}}^{+} \mathrm{e}^{\mathrm{i}k_y^m y} \mathrm{e}^{\mathrm{i}k_x x} & y > d \\ \int \mathrm{d}k_x S_d (B_{\mathrm{TM}}^{+} \mathrm{e}^{\mathrm{i}k_y^d y} - B_{\mathrm{TM}}^{-} \mathrm{e}^{-\mathrm{i}k_y^d y}) \mathrm{e}^{\mathrm{i}k_x x} & -d < y < d. \\ \int \mathrm{d}k_x (-S_g C_{\mathrm{TM}}^{-} \mathrm{e}^{\mathrm{i}k_y^g y} \mathrm{e}^{\mathrm{i}k_x x}) & y < -d \end{cases} \tag{4}$$

Here, $B_{\mathrm{TM}}^{\pm}$ and $C_{\mathrm{TM}}^{\pm}$ represent reflection coefficients and transmission coefficients of the transverse magnetic field, and their superscripts + and − denote the upper interface and lower interface, respectively. Meanwhile, $S_d = \frac{k_y^d}{\varepsilon_d}$, $S_m = \frac{k_y^m}{\varepsilon_m}$, $S_g = \frac{\varepsilon_t k_y^g - (\mathrm{i}\varepsilon_g)k_x}{\varepsilon_t^2 + (\mathrm{i}\varepsilon_g)^2}$, k_x is the wavevector along x direction, $k_y^d = \sqrt{\epsilon_d k_0^2 - k_x^2}$, $k_y^m = \sqrt{\epsilon_m k_0^2 - k_x^2}$, and $k_y^g = \sqrt{\epsilon_{\mathrm{eff}} k_0^2 - k_x^2}$ (k_0 is the wavevector of the incident light in free space). The effective permittivity of the gyrotropic material can be obtained as $\varepsilon_{\mathrm{eff}} = \frac{\varepsilon_t^2 + (\mathrm{i}\varepsilon_g)^2}{\varepsilon_t}$. The continuity of the tangent field components (i.e., H_z^f and E_z^f) cancels out all the reflection and transmission coefficients, so that the eigenmode equation can be derived as

$$\mathrm{e}^{4\mathrm{i}k_y^d d} = \frac{(S_g + S_d)(S_m + S_d)}{(S_m - S_d)(S_g - S_d)}. \tag{5}$$

Then, we assume that a linearly polarized emitter with x-oriented dipole momentum of p_e is placed on the center of the waveguide. The H_z component and E_x component of the dipole source within the dielectric slab ($-d < y < d$) can be expressed as [11]

$$H_z^s = \int \mathrm{d}k_x A \mathrm{e}^{\mathrm{i}k_y^d |y|} \mathrm{e}^{\mathrm{i}k_x x}, \tag{6}$$

$$E_x^s = -\frac{1}{\omega\varepsilon_0}\int \mathrm{d}k_x S_d[\mathrm{sgn}(y) A \mathrm{e}^{\mathrm{i}k_y^d |y|}] \mathrm{e}^{\mathrm{i}k_x x}. \tag{7}$$

Finally, components of the total field are combined as

$$H_z^t = H_z^f + H_z^s, \tag{8}$$

$$E_x^t = E_x^f + E_x^s, \tag{9}$$

respectively. In this case, the reflection coefficients $B_{\mathrm{TM}}^{\pm}$ and the transmission coefficients $C_{\mathrm{TM}}^{\pm}$ are determined by matching the boundary conditions of the total field (i.e., the continuity of E_x^t and H_z^t) as

$$B^{+}_{\mathrm{TM}} = \frac{(S_d - S_m)(S_g - S_d)\mathrm{e}^{2\mathrm{i}k_y^d d} - (S_d - S_g)(S_m + S_d)}{(S_m - S_d)(S_g - S_d)\mathrm{e}^{2\mathrm{i}k_y^d d} - (S_g + S_d)(S_m + S_d)\mathrm{e}^{-2\mathrm{i}k_y^d d}} A, \tag{10}$$

$$B^{-}_{\mathrm{TM}} = \frac{(S_d - S_m)(S_g - S_d)\mathrm{e}^{2\mathrm{i}k_y^d d} - (S_d - S_m)(S_g + S_d)}{(S_m - S_d)(S_g - S_d)\mathrm{e}^{2\mathrm{i}k_y^d d} - (S_g + S_d)(S_m + S_d)\mathrm{e}^{-2\mathrm{i}k_y^d d}} A, \tag{11}$$

$$C^{+}_{\mathrm{TM}} = B^{+}_{\mathrm{TM}}\mathrm{e}^{\mathrm{i}(k_y^d - k_y^m)d} + B^{-}_{\mathrm{TM}}\mathrm{e}^{-\mathrm{i}(k_y^d + k_y^m)d} + A\mathrm{e}^{\mathrm{i}(k_y^d - k_y^m)d}, \tag{12}$$

$$C^{-}_{\mathrm{TM}} = B^{+}_{\mathrm{TM}}\mathrm{e}^{-\mathrm{i}(k_y^d + k_y^g)d} + B^{-}_{\mathrm{TM}}\mathrm{e}^{\mathrm{i}(k_y^d - k_y^g)d} + A\mathrm{e}^{\mathrm{i}(k_y^d - k_y^g)d}. \tag{13}$$

Here, $A = -\frac{\mathrm{i}\omega p_c k_x}{4\pi k_y^d}$ is the amplitude of the dipole source.

3. RESULTS AND DISCUSSION

As shown in Fig. 1(b), without the static magnetic field (the cyclotron frequency $\omega_c = 0$), the dispersion relations of the guiding modes are symmetric with two branches. They are, respectively, odd modes (blue line) and even modes (red line) induced by the strong coupling between the SPPs at adjacent interfaces [27]. We notice that the odd modes have a positive equivalent refractive index ($n_{\mathrm{eff}} > 0$), and the corresponding energy flux propagates parallel to the wavevector of the SPPs, whereas the energy flux and the wavevector are antiparallel to each other for the even modes whose equivalent refractive index is negative.

By introducing a non-zero static magnetic field in the gyrotropic material, the symmetric dispersion relations shown in Fig. 2(a) are broken, which leads to a unidirectional emission of the dipole. In fact, the directionality of the EM modes is determined mainly by the dominant mode confined on the structure and the sign of the corresponding equivalent refractive index n_{eff}. Accordingly, we classify the operation wavebands as channel 1, channel 2, channel 3, and channel 4, respectively, showing different nonreciprocal behaviors. The corresponding emission field is given in Fig. 2(b), calculated by Eqs. (8)–(13). In channel 1, the dipole source emits both forward ($+x$ direction) and backward ($-x$ direction) EM modes. However, when $k_x > 0$, the dispersion curve is closer to the light line. Therefore, the EM field with a positive wavevector is weakly confined in the waveguide, resulting in a fast decay in free space. Owing to the direction of the energy flux coinciding with that of the wavevector ($n_{\mathrm{eff}} > 0$), the backward emission is dominant [see Fig. 2(biv)]. Although the EM field in channel 4 is confined more effectively in the waveguide when $k_x > 0$, the negative n_{eff} implies that the EM modes of the positive wavevector are mainly backward propagating [see Fig. 2(bi)]. It is also seen that channel 2 supports only the EM mode of the positive wavevector, while the EM modes of the negative wavevector are supported only in channel 3. Due to the opposite sign of the n_{eff} in these two situations, the emission of the dipole is routed forward in channels 2 and 3 [see Figs. 2(bii) and 2(biii)].

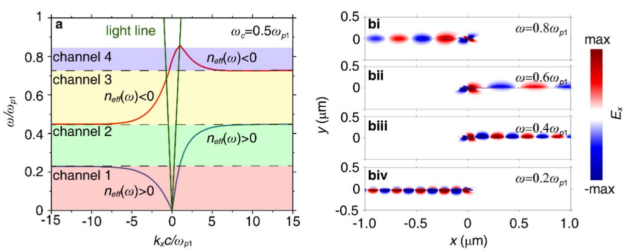

Fig. 2. (a) Dispersion relation of the multi-channel nonreciprocal waveguide when the cyclotron frequency $\omega_c = 0.5\omega_{p1}$ (non-zero magnetic field). There are four non-reciprocal channels, as highlighted in different colors. (bi)–(biv) Field distributions in the four nonreciprocal channels. In each nonreciprocal channel, photons from the dipole are emitted in a nonreciprocal manner.

The directionalities of the nonreciprocal waveguide in different waveband channels are evaluated and shown in Fig. 3. The forward and backward directionalities are determined by Eqs. (14) and (15), respectively:

$$D_1 = \frac{P_L(\omega)}{P_{-L}(\omega) + P_L(\omega)}, \tag{14}$$

$$D_2 = \frac{P_{-L}(\omega)}{P_{-L}(\omega) + P_L(\omega)}, \tag{15}$$

in which $P_L(\omega)$ [$P_{-L}(\omega)$] denotes the power density harvested at the distance of L ($-L$) away from the dipole source. It is shown that the directionality is around 95% in channel 1 and over 70% in channel 4. However, the directionalities of these two channels are lower than those in channels 2 and 3 (the directionalities in channels 2 and 3 are 100%) because in channels 1 and 4, the EM emissions are weakly unidirectional, while in channels 2 and 3, the EM emissions are truly unidirectional.

To demonstrate the separation of high-order harmonic from the fundamental signal in our proposed multi-channel nonreciprocal waveguide, we replace the transparent dielectric by a second-order nonlinear material with the nonlinear susceptibility $\chi^{(2)} = 2$ pm/V. We implement the nonlinear model by COMSOL Multiphysics 5.3a. The method of undepleted pump approximation is used to simplify the problem, assuming that the nonlinear polarization is much smaller than the linear

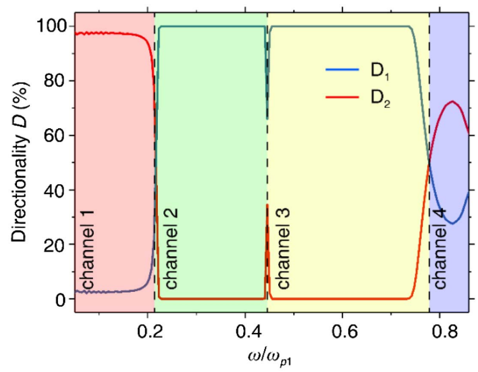

Fig. 3. Calculated directionality of each nonreciprocal channel. D_1 is the forward directionality (blue line), and D_2 is the backward directionality (red line). Different channels are highlighted in different colors as in Fig. 2(a).

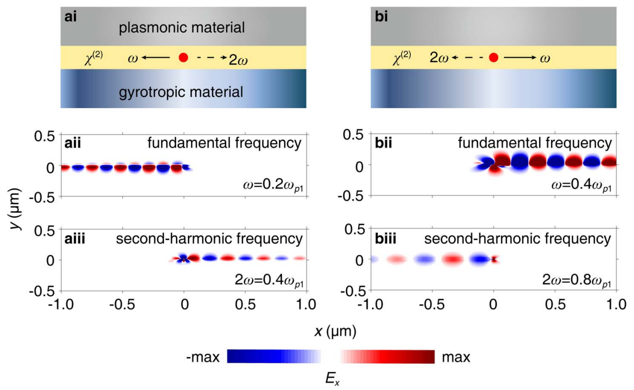

Fig. 4. Two schemes to separate the fundamental signal and the second harmonic using the multi-channel nonreciprocal waveguide. (ai) Schematic diagram of the first scheme: the fundamental signal in channel 1 is routed backward [see (aii)], while the second harmonic in channel 2 is routed forward [see (aiii)]. (bi) Schematic diagram of the second scheme: the fundamental signal in channel 2 is routed forward [see (bii)], while the second harmonic in channel 4 is routed backward [see (biii)].

polarization. Under this assumption, we obtain the second-harmonic field E_{SHG} generated by the defined external current as $J_{\mathrm{ext}} = \mathrm{i}2\omega\chi^{(2)}E_{\mathrm{FF}}^2$, where E_{FF} is the fundamental electric field [28,29]. When the fundamental signal is propagated mainly along the $-x$ direction (backward) with the frequency $\omega = 0.2\omega_{p1}$ in channel 1, the generated second harmonic with frequency $2\omega = 0.4\omega_{p1}$ is totally propagated along the $+x$ direction (forward) in channel 2 [see Fig. 4(a)]. In contrast, when the fundamental signal with the frequency $\omega = 0.4\omega_{p1}$ in channel 2 is propagated along the $+x$ direction (forward), the induced second harmonic with frequency $2\omega = 0.8\omega_{p1}$ is emitted mainly in the $-x$ direction (backward) in channel 4 [see Fig. 4(b)].

Figure 5 shows the power spectra of the fundamental signal (blue line) and the induced second harmonic (red line) corresponding to the above two schemes. For the first scheme, the power of the second harmonic reaches a maximum value of 8.8×10^{-5} W/m when the fundamental frequency is $\omega = 0.177\omega_{p1}$. But it vanishes when the operation frequency is beyond the cutoff frequency of channel 1. In the second scheme, the induced second harmonic has a peak power value of 1.65×10^{-5} W/m when the fundamental frequency is $\omega = 0.42\omega_{p1}$. However, the operation bandwidth of the second harmonic is

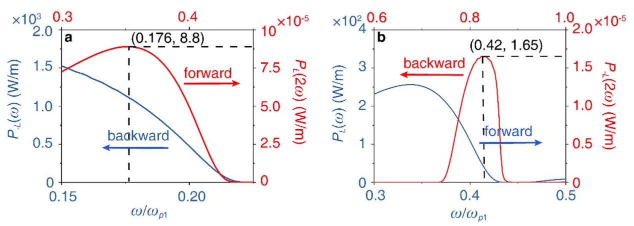

Fig. 5. Calculated power density of the fundamental signal (blue line) and the second harmonic (red line) at $L = 1$ μm away from the dipole source in (a) the first scheme and (b) the second scheme, as indicated in Fig. 4. The arrows represent the propagation direction of the corresponding EM modes.

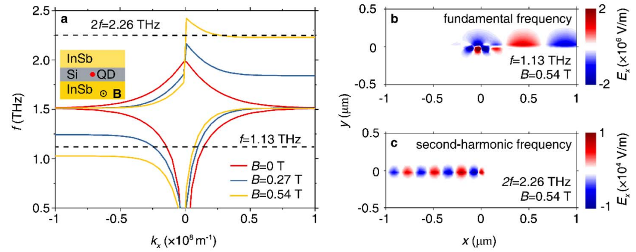

Fig. 6. (a) Dispersion relations of a realistic structure, where both the plasmonic material and the gyrotropic material are doped InSb, and the dielectric is replaced by the strained Si. The QD is embedded in the Si slab. A static magnetic field is applied on the InSb in the bottom layer, shown as the inset. For comparison, dispersion relations are plotted for the system under the static magnetic field $B = 0$ T, $B = 0.27$ T, and $B = 0.54$ T, respectively. (b), (c) Field distributions in the fundamental frequency and in the second-harmonic frequency bands under the static magnetic field $B = 0.54$ T, respectively.

limited by the narrow operation waveband of channel 4. Moreover, we unveil that the second harmonic generated by the first scheme is more effective than that induced by the second scheme. This is attributed mainly to the weaker directionality of channel 4 than that of channel 1.

Finally, we present a possibility to construct such a multi-channel nonreciprocal waveguide using doped indium antimonide (InSb) and strained silicon (Si), shown as the inset in Fig. 6(a). The InSb in the top layer behaves as a plasmonic material in the terahertz frequency band [30]. Under the static magnetic field, the InSb in the bottom layer exhibits the features of gyrotropic material. The critical optical parameters of the InSb are obtained from Ref. [6] (i.e., $\epsilon_\infty = 15.6$, and $\omega_p = 4\pi \times 10^{12}$ rad/s). The cyclotron frequency of the InSb is determined by $\omega_c = \frac{eB}{m^*}$, where the effective mass of the InSb $m^* = 0.0126m_0$ (e is the unit of the electron charge, and m_0 is the remaining mass of the electron) [31]. Moreover, the thickness of the Si slab in the center is $2d = 50$ nm, relative permittivity of the Si is $\epsilon_d = 11.68$, and second-order susceptibility of the Si is selected as $\chi^{(2)} = 2$ pm/V, which can be tuned with different strain levels [32]. With the static magnetic field enhanced from 0 to 0.54 T, the waveguide system shows increasing nonreciprocity in the terahertz frequency band, and the wavebands of working channels are changed accordingly [see Fig. 6(a)]. This allows the design of photonic dichroism in the terahertz frequency band flexibly. For instance, if $B = 0.54$ T, the quantum dot (QD) with the frequency of 1.13 THz can emit light only in the forward direction, while its second harmonic is routed backward [see Fig. 6(b)].

4. CONCLUSION

In conclusion, we proposed a four-channel nonreciprocal waveguide composed of a plasmonic material layer, a transparent dielectric layer, and a gyrotropic material layer. We have shown rigorously that the emission of the dipole source can be unidirectionally routed at will by controlling the operation frequency of the proposed waveguide. Notably, truly unidirectional emission is realized in channels 2 and 3, whereas weakly unidirectional emission occurs in other channels. We anticipate that additional unidirectional coupling could be observed in similar waveguide structures if the linear dipole is replaced by a spinning dipole [33,34]. The associated spin-orbit interaction can also bring intriguing effects, such as spin-Hall effect of light [35,36], which is a promising way to precisely locate nanoparticles or probe local optical fields. In addition, our numerical results unambiguously reveal that the high-order harmonic from the fundamental signal is separated during the nonlinear process by applying the multi-channel nonreciprocal waveguide. Our proposed multi-channel nonreciprocal waveguide offers significant guidance for the design of novel photonic dichroism with a tunable waveband, high integration, and multiple channels.

Funding. National Natural Science Foundation of China (NSFC) (11504252, 61701246); Natural Science Research of Jiangsu Higher Education Institutions of China (17KJB140014); Natural Science Foundation of Jiangsu Province (BK20150306); China Postdoctoral Science Foundation (2018M630596); Priority Academic Program Development of Jiangsu Higher Education Institutions; Ministry of Education - Singapore (MOE) (2017-T1-001-239 (RG91/17 (S)), MOE2015-T2-1-145).

REFERENCES

1. W. Y. Yin and W. Wan, "Radiation from a dipole in the presence of a grounded arbitrary magnetized chiroferrite slab," Int. J. Infrared Millim. Waves **15**, 1263–1274 (1994).
2. P. S. Epstein, "Theory of wave propagation in a gyromagnetic medium," Rev. Mod. Phys. **28**, 3–17 (1956).
3. C. W. Qiu, H. Y. Yao, L. W. Li, S. Zouhdi, and T. S. Yeo, "Routes to left-handed materials by magnetoelectric couplings," Phys. Rev. B **75**, 245214 (2007).
4. E. Cojocaru, "Modes in dielectric or ferrite gyrotropic slab and circular waveguides, longitudinally magnetized, with open and completely or partially filled wall," J. Opt. Soc. Am. B **27**, 1965–1977 (2010).
5. F. Fan, S. Chen, X. H. Wang, and S. J. Chang, "Tunable nonreciprocal terahertz transmission and enhancement based on metal/magneto-optic plasmonic lens," Opt. Express **21**, 8614–8621 (2013).
6. K. L. Tsakmakidis, L. Shen, S. A. Schulz, X. Zheng, J. Upham, X. Deng, H. Altug, A. F. Vakakis, and R. W. Boyd, "Breaking Lorentz reciprocity to overcome the time-bandwidth limit in physics and engineering," Science **356**, 1260–1264 (2017).
7. X. Lin, Z. J. Wang, F. Gao, B. L. Zhang, and H. S. Chen, "Atomically thin nonreciprocal optical isolation," Sci. Rep. **4**, 4190 (2014).
8. T. S. Qiu, J. Wang, Y. F. Li, and S. B. Qu, "Circulator based on spoof surface plasmon polaritons," IEEE Antennas Wireless Propag. Lett. **16**, 821–824 (2017).
9. Z. Wang, Y. D. Chong, J. D. Joannopoulos, and M. Soljacic, "Observation of unidirectional backscattering-immune topological electromagnetic states," Nature **461**, 772–775 (2009).
10. C. He, X. C. Sun, X. P. Liu, M. H. Lu, Y. Chen, L. Feng, and Y. F. Chen, "Photonic topological insulator with broken time-reversal symmetry," Proc. Natl. Acad. Sci. USA **113**, 4924–4928 (2016).
11. F. R. Prudencio and M. G. Silveirinha, "Asymmetric Cherenkov emission in a topological plasmonic waveguide," Phys. Rev. B **98**, 115136 (2018).
12. S. A. Gangaraj, G. W. Hanson, M. G. Silveirinha, K. Shastri, M. Antezza, and F. Monticone, "Truly unidirectional excitation and propagation of diffractionless surface plasmon-polaritons," arXiv: 1811.00463 (2018).
13. H. Hu, J. L. Zhang, S. A. Maier, and Y. Luo, "Enhancing third-harmonic generation with spatial nonlocality," ACS Photon. **5**, 592–598 (2018).
14. S. Hou, A. Xie, Z. Xie, L. Y. M. Tobing, J. Zhou, L. Tjahjana, J. Yu, C. Hettiarachchi, D. Zhang, C. Dang, E. H. T. Teo, M. D. Birowosuto, and H. Wang, "Concurrent inhibition and redistribution of spontaneous emission from all inorganic perovskite photonic crystals," ACS Photon. (2019), DOI: 10.1021/acsphotonics.8b01655.
15. J. Y. Yin, J. Ren, H. C. Zhang, B. C. Pan, and T. J. Cui, "Broadband frequency-selective spoof surface plasmon polaritons on ultrathin metallic structure," Sci. Rep. **5**, 8165 (2015).
16. L. L. Liu, Z. Li, B. Z. Xu, C. Q. Gu, X. L. Chen, H. Y. Sun, Y. J. Zhou, Q. Qing, P. Shum, and Y. Luo, "Ultra-low-loss high-contrast gratings based spoof surface plasmonic waveguide," IEEE Trans. Microwave Theory Tech. **65**, 2008–2018 (2017).
17. Z. F. Yu, G. Veronis, Z. Wang, and S. H. Fan, "One-way electromagnetic waveguide formed at the interface between a plasmonic metal under a static magnetic field and a photonic crystal," Phys. Rev. Lett. **100**, 023902 (2008).
18. Y. Kurokawa and H. T. Miyazaki, "Metal-insulator-metal plasmon nanocavities: analysis of optical properties," Phys. Rev. B **75**, 035411 (2007).
19. S. R. K. Rodriguez, "Classical and quantum distinctions between weak and strong coupling," Eur. J. Phys. **37**, 025802 (2016).
20. S. F. Lan, L. Kang, D. T. Schoen, S. P. Rodrigues, Y. H. Cui, M. L. Brongersma, and W. S. Cai, "Backward phase-matching for nonlinear optical generation in negative-index materials," Nat. Mater. **14**, 807–811 (2015).
21. A. K. Popov, I. S. Nefedov, and S. A. Myslivets, "Hyperbolic carbon nanoforest for phase matching of ordinary and backward electromagnetic waves: second harmonic generation," ACS Photon. **4**, 1240–1244 (2017).
22. G. X. Li, L. Wu, K. F. Li, S. M. Chen, C. Schlickriede, Z. J. Xu, S. Y. Huang, W. D. Li, Y. J. Liu, E. Y. B. Pun, T. Zentgraf, K. W. Cheah, Y. Luo, and S. Zhang, "Nonlinear metasurface for simultaneous control of spin and orbital angular momentum in second harmonic generation," Nano Lett. **17**, 7974–7979 (2017).
23. L. L. Liu, L. Wu, J. J. Zhang, Z. Li, B. L. Zhang, and Y. Luo, "Backward phase matching for second harmonic generation in negative-index conformal surface plasmonic metamaterials," Adv. Sci. **5**, 1800661 (2018).
24. X. P. Hu, P. Xu, and S. N. Zhu, "Engineered quasi-phase-matching for laser techniques," Photon. Res. **1**, 171–185 (2013).
25. A. Eroglu, *Wave Propagation and Radiation in Gyrotropic and Anisotropic Media* (Springer, 2010), p. 31.
26. J. X. Huang, H. Hu, Z. W. Wang, W. Y. Li, J. Cang, J. Q. Shen, and H. Ye, "Analysis of light-emission enhancement of low-efficiency quantum dots by plasmonic nano-particle," Opt. Express **24**, 8555–8573 (2016).
27. J. Tao, Q. J. Wang, J. J. Zhang, and Y. Luo, "Reverse surface-polariton Cherenkov radiation," Sci. Rep. **6**, 30704 (2016).
28. L. Carletti, A. Locatelli, O. Stepanenko, G. Leo, and C. De Angelis, "Enhanced second-harmonic generation from magnetic resonance in AlGaAs nanoantennas," Opt. Express **23**, 26544–26550 (2015).
29. M. Celebrano, X. F. Wu, M. Baselli, S. Grossmann, P. Biagioni, A. Locatelli, C. De Angelis, G. Cerullo, R. Osellame, B. Hecht, L. Duo, F. Ciccacci, and M. Finazzi, "Mode matching in multiresonant plasmonic nanoantennas for enhanced second harmonic generation," Nat. Nanotechnol. **10**, 412–417 (2015).
30. S. M. Hanham, A. I. Fernandez-Dominguez, J. H. Teng, S. S. Ang, K. P. Lim, S. F. Yoon, C. Y. Ngo, N. Klein, J. B. Pendry, and S. A. Maier, "Broadband terahertz plasmonic response of touching InSb disks," Adv. Mater. **24**, Op226–Op230 (2012).
31. J. R. Maack, N. A. Mortensen, and M. Wubs, "Size-dependent nonlocal effects in plasmonic semiconductor particles," Europhys. Lett. **119**, 17003 (2017).
32. M. Cazzanelli, F. Bianco, M. Ghulinyan, G. Pucker, D. Modotto, S. Wabnitz, F. M. Pigozzo, S. Ossicini, E. Degoli, E. Luppi, V. Veniard, and L. Pavesi, "Second-order nonlinear silicon photonics," SPIE Newsroom (2012), DOI: 10.1117/2.1201203.004138.
33. L. Marrucci, "Spin gives direction," Nat. Phys. **11**, 9–10 (2015).
34. F. J. Rodríguez-Fortuño, G. Marino, P. Ginzburg, D. O'Connor, A. Martínez, G. A. Wurtz, and A. V. Zayats, "Near-field interference for the unidirectional excitation of electromagnetic guided modes," Science **340**, 328–330 (2013).
35. D. Gao, R. Shi, A. E. Miroshnichenko, and L. Gao, "Enhanced spin Hall effect of light in spheres with dual symmetry," Laser Photon. Rev. **12**, 1800130 (2018).
36. R. Shi, D. L. Gao, H. Hu, Y. Q. Wang, and L. Gao, "Enhanced broadband spin Hall effects by core-shell nanoparticles," Opt. Express **27**, 4808–4817 (2019).